Collimator design for a dedicated molecular breast imaging-guided biopsy system: Proof-of-concept

Amanda L. Weinmann, Carrie B. Hruska,[a] Amy L. Conners, and Michael K. O'Connor
Department of Radiology, Mayo Clinic, 200 First Street SW, Rochester, Minnesota 55905

(Received 7 June 2012; revised 13 November 2012; accepted for publication 15 November 2012; published 17 December 2012)

Purpose: Molecular breast imaging (MBI) is a dedicated nuclear medicine breast imaging modality that employs dual-head cadmium zinc telluride (CZT) gamma cameras to functionally detect breast cancer. MBI has been shown to detect breast cancers otherwise occult on mammography and ultrasound. Currently, a MBI-guided biopsy system does not exist to biopsy such lesions. Our objective was to consider the utility of a novel conical slant-hole (CSH) collimator for rapid (<1 min) and accurate monitoring of lesion position to serve as part of a MBI-guided biopsy system.
Methods: An initial CSH collimator design was derived from the dimensions of a parallel-hole collimator optimized for MBI performed with dual-head CZT gamma cameras. The parameters of the CSH collimator included the collimator height, cone slant angle, thickness of septa and cones of the collimator, and the annular areas exposed at the base of the cones. These parameters were varied within the geometric constraints of the MBI system to create several potential CSH collimator designs. The CSH collimator designs were evaluated using Monte Carlo simulations. The model included a breast compressed to a thickness of 6 cm with a 1-cm diameter lesion located 3 cm from the collimator face. The number of particles simulated was chosen to represent the count density of a low-dose, screening MBI study acquired with the parallel-hole collimator for 10 min after a ~150 MBq (4 mCi) injection of Tc-99m sestamibi. The same number of particles was used for the CSH collimator simulations. In the resulting simulated images, the count sensitivity, spatial resolution, and accuracy of the lesion depth determined from the lesion profile width were evaluated.
Results: The CSH collimator design with default parameters derived from the optimal parallel-hole collimator provided 1-min images with error in the lesion depth estimation of 1.1 ± 0.7 mm and over 21 times the lesion count sensitivity relative to 1-min images acquired with the current parallel-hole collimator. Sensitivity was increased via more vertical cone slant angles, larger annular areas, thinner cone walls, shorter cone heights, and thinner radiating septa. Full width at half maximum trended in the opposite direction as sensitivity for all parameters. There was less error in the depth estimates for less vertical slant angles, smaller annular areas, thinner cone walls, cone heights near 1 cm, and generally thinner radiating septa.
Conclusions: A Monte Carlo model was used to demonstrate the feasibility of a CSH collimator design for rapid biopsy application in molecular breast imaging. Specifically, lesion depth of a 1-cm diameter lesion positioned in the center of a typical breast can be estimated with error of less than 2 mm using circumferential count profiles of images acquired in 1 min. [http://dx.doi.org/10.1118/1.4770274]

Key words: molecular breast imaging, collimator, biopsy

I. INTRODUCTION

For over a decade, a number of laboratories have worked to develop dedicated nuclear medicine technologies that rely on the preferential accumulation of an intravenously injected radiotracer in malignant cells to detect breast cancer. These technologies include those that detect ^{18}F-fluorodeoxyglucose (FDG) positron emissions such as positron emission mammography (PEM) and others that utilize single-photon emitting radiotracers (typically Tc-99m sestamibi) such as breast-specific gamma imaging (BSGI) and molecular breast imaging (MBI).[1–3] All of these dedicated technologies use small detectors with minimal dead space at the detector edge, permitting the breast to be placed in direct contact with the detector head, thereby allowing high spatial resolution imaging of small breast tumors.

Clinical studies evaluating these nuclear medicine technologies have demonstrated their ability to detect breast cancer occult on the traditional modalities of mammography and ultrasound in the setting of screening asymptomatic women[4–6] and in the setting of screening for additional disease as part of presurgical evaluation.[7,8] Work from our laboratory has focused on MBI performed with a dual-head cadmium zinc telluride (CZT) detector and has demonstrated its potential to be a useful breast cancer screening modality. In women with mammographically dense breasts, MBI performed as an adjunct to screening mammography increased cancer detection sensitivity to 91% from 27% for

mammography alone ($p = 0.016$).[4] Because MBI has the ability to reveal mammographically occult breast lesions, it is important that there be a feasible way to biopsy suspicious new MBI findings.

The diagnostic algorithm used at our institution recommends that a positive MBI study (as defined by the current MBI lexicon[9]) be worked up with diagnostic mammogram and/or targeted ultrasound. Most MBI-detected lesions are either deemed to be benign on work-up or after short-term MBI follow-up, or are subsequently biopsied using ultrasound-guided core-needle biopsy, a relatively straightforward and inexpensive procedure. If the diagnostic mammogram and ultrasound are not able to resolve the findings, breast magnetic resonance (MR) imaging may be indicated, in which case a MR-guided biopsy may be performed if warranted.

Of the patients who have a diagnostic evaluation prompted by a positive MBI, approximately 12% go on to have a MR-guided biopsy.[10] Despite its diagnostic utility, dependence on MR-guided biopsy to resolve MBI-detected lesions is untenable because it is not available at all institutions and is considerably more expensive, technically challenging, and time-consuming than other biopsy methods. In addition, some patients have contraindications to MR imaging such as implantable devices or an inability to tolerate the procedure.[11]

The demonstrated ability of MBI to detect mammographically and sonographically occult breast cancers and the challenges and cost associated with MR-guided biopsy underscore the need for a simple, rapid MBI-guided biopsy system. Early work in the field of scintimammography suggested that nuclear medicine technologies could guide breast biopsy,[12–15] and more recently, biopsy devices have been developed for both PEM and BSGI.[16,17] To date, a comparable biopsy system has not been developed for MBI.

This paper describes a novel collimator for use in rapidly localizing a lesion as part of a MBI-guided biopsy system. The aim of this work was to evaluate the feasibility of a collimator design that (1) permits accurate determination of lesion depth for biopsy guidance and (2) improves lesion count sensitivity to enable rapid monitoring of lesion location throughout the biopsy procedure.

II. METHODS AND SIMULATION

II.A. Molecular breast imaging procedure

MBI employs two opposed CZT-based gamma cameras to obtain planar images of the breast in a configuration similar to mammography (Fig. 1). In our current practice, the patient typically receives an intravenous injection of ~300 MBq (8 mCi) Tc-99m sestamibi, and imaging commences approximately 5 min postinjection. The patient is seated with her breast lightly compressed between the two gamma cameras, and radiation emitted by Tc-99m sestamibi is detected after collimation. Four 10-min views are acquired: a craniocaudal and a mediolateral oblique image of each breast, similar to those obtained in mammography.

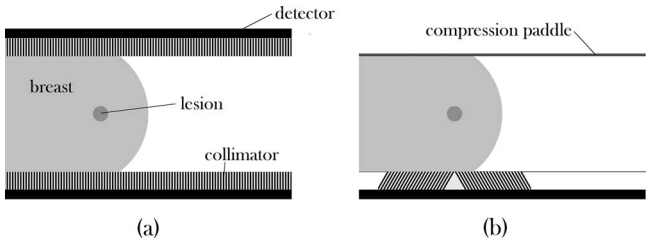

FIG. 1. Side-view diagrams of (a) a standard MBI setup with a lesion within a breast that is lightly compressed between two heads, each consisting of a collimator and detector, and (b) the proposed biopsy setup with one detector and collimator unit replaced with a compression paddle and the other collimator replaced with the conical slant-hole collimator as described in the text.

II.B. Design considerations for MBI-guided biopsy

The two main design considerations for a clinically feasible biopsy system are (1) the ability to localize the lesion in three dimensions, and (2) the ability to rapidly acquire images during the procedure, allowing guidance of the biopsy needle.

The MBI system in its current dual-head configuration allows localization in two dimensions from a single planar image, but additional calculations must be performed to determine the distance of the lesion from the collimator surfaces (i.e., depth within the breast). Previous work on the quantification of Tc99m-sestamibi uptake in MBI-detected lesions has shown that lesion depth can be estimated to within 1 mm using the ratio of counts in the conjugate views of the breast acquired from the opposed detectors.[18] However, the use of a dual-head system with the breast compressed between the two detectors substantially limits a radiologist's access to the breast for the biopsy procedure. In this work, we propose a design where one of the detectors is replaced with a compression paddle, thus reducing the MBI-guided biopsy system to a single-detector system (Fig. 1), which would allow for improved access to the breast. As a result of a single-detector biopsy system, the previously mentioned quantification method cannot be used since depth information cannot be calculated from a single detector with parallel-hole collimation.

Additionally, the previously mentioned quantification method is also limited in the clinical biopsy setting, as the time needed to obtain a typical MBI image is too long for biopsy purposes (10 min/view). Ideally, localization should be done in real-time to monitor patient and lesion movement throughout the biopsy procedure. Given the limited count flux available in MBI studies, a more practical goal is to acquire images in 1 min or less. We selected a 1 min imaging time as an acceptable tradeoff in the clinical setting that would allow relatively rapid updates of needle and lesion position during the procedure and still provide adequate count sensitivity for accurate depth localization. A MBI image acquired in 1 min with the current parallel-hole, high sensitivity collimator design is expected to be too noisy to be useful for biopsy purposes.

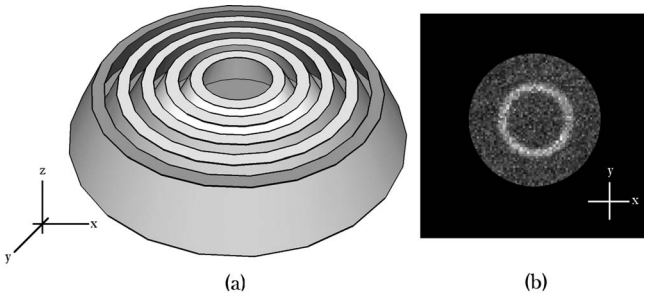

FIG. 2. (a) Illustration of a conceptualized conical slant-hole collimator constructed from concentric truncated cones, with (b) a hypothetical image of a single lesion acquired using such a collimator.

II.C. Theoretical conical collimator design

To address the above limitations, we modified the traditional parallel-hole collimator design. To triangulate depth information, the collimator holes were designed as slanted rather than parallel. Slant-hole collimation, by itself, is not a novel design and is used to calculate lesion depth in the BSGI biopsy system.[17] Though slant-hole collimation provides the ability to triangulate lesion depth, it only yields about a twofold gain in sensitivity, prohibiting rapid imaging. Hence, to further improve sensitivity, the slanted collimator holes were arranged in a circle to maximize the detection of photons originating from the lesion. This design resulted in a theoretical collimator of concentric truncated cones, from here on referred to as a conical slant hole (CSH) collimator.

The resulting image from a CSH collimator design would theoretically be a ring of increased uptake originating from the lesion, superimposed on a disc of background activity from surrounding breast tissue (Fig. 2). The ring of increased intensity allows summation of counts in the radial profile to increase lesion count sensitivity, and the depth of a lesion can be calculated from the diameter of the ring. One obvious requirement of this design is that the collimator must be centered relative to the lesion. This adjustability can be achieved by making the collimator smaller than the field-of-view and by placing it on a movable platform with shielding surrounding the collimator.

II.D. Monte Carlo simulations

The parallel-hole collimator currently used with the MBI system and a theoretical CSH collimator design were simulated using Monte Carlo modeling with Monte Carlo n-particle (MCNP) code, Version 5 (Los Alamos National Laboratory).[19] This Monte Carlo simulation has been previously validated in our laboratory; comparisons of measured spatial resolution and count sensitivity measured from simulated images were within an average of 1.5% different from the theoretical values.[20] All of the simulations modeled the same gamma detector and breast tissue containing a lesion. Only the collimator characteristics varied between simulations.

To reduce the number of necessary simulations and because our intent was solely to evaluate the feasibility of the CSH collimator design, only one of the two types of CZT detectors used in our laboratory was considered. This detector was the LumaGEM (Gamma Medica-Ideas, Northridge, CA) consisting of a 96×128 array of $1.6 \times 1.6 \times 5.0$ mm^3 CZT elements, yielding a total field-of-view of $\sim 15 \times 20$ cm^2.

A 6 cm thick breast (approximating the average thickness of the lightly compressed breast observed in MBI imaging[3,21]) was simulated with a uniform density of 1.0 g/cm^3. A tumor was simulated with a diameter of 1 cm, which is representative of the mammographically occult invasive cancers that have been observed in a screening population with MBI (median diameter 1.1 cm).[4] The typical depth of lesions is unknown, so a depth of 3 cm was used, corresponding to the furthest distance from either of the dual-head detectors. The tumor-to-background ratio was simulated as 20:1,[22] and the energy acceptance window was set to 110–154 keV.[23]

The number of particles generated was chosen so that simulations of the registered high-sensitivity MBI collimator (described below) generated images with background tissue count densities similar to what is observed clinically in patient MBI studies (median: 4.60 ± 1.13 counts/cm^2/10 min/MBq).[24] Currently, we employ an administered dose of $\sim$300 MBq Tc-99m sestamibi, with a goal of reducing this dose to 150 MBq in the screening setting. Hence, the simulations were designed to achieve a count density of approximately 690 ± 170 counts/cm^2, equivalent to the theoretical mean count density in a patient image acquired for 10 min with an administered dose of 150 MBq sestamibi. The number of particles that must be simulated to produce this count density in a MBI image obtained using the previously mentioned parallel-hole collimator was established, and that same number of particles was used when simulating the CSH collimators. One-min images were created by reconstructing frames of the simulated list-mode data.

II.E. Parallel-hole collimator simulations

We first simulated MBI images acquired using the LumaGEM CZT detector and the parallel-hole registered collimator that was developed in our laboratory.[20] This collimator is a tungsten square-hole collimator with hole length 0.94 cm, septal thickness 0.375 mm, and hole width 1.225 mm. This design yields a unit pitch of 1.6 mm, and the collimator is positioned on the detector such that each hole is registered with an element of the CZT detector. The collimator is constructed of tungsten rather than lead so that the septal walls are thinner to achieve the greatest sensitivity with the registered 1.6 mm unit pitch.

II.F. Conical slant-hole collimator simulations

Five variables that influence the performance of the CSH collimator were examined: (a) the slant angle of the cones, (b) distance between cones, (c) cone wall thickness, (d) cone height, and (e) the presence and shape of radial septa (Fig. 3). The relationship between these variables could not be

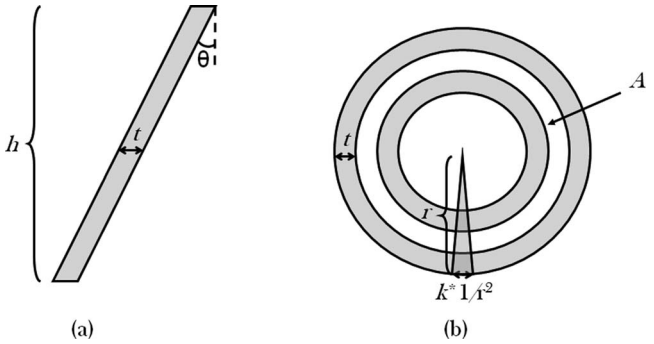

FIG. 3. (a) Side and (b) top view diagrams demonstrating the five parameters that were varied in the conical slant-hole collimator simulations. h is the height of the collimator; t is the cone wall thickness; θ is the slant angle as measured from vertical; A is the annular area of uncovered detector surface between the cones; and k is a coefficient describing the outer thicknesses of the radiating wedge-shaped septa.

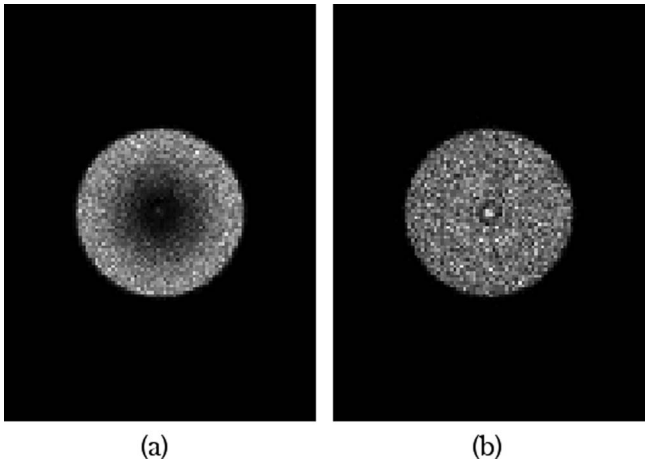

FIG. 4. Simulated images of a background, nonlesion containing phantom. The images were acquired with identical conical slant-hole collimators, with the exception of one having equally spaced cones (a) and the other having cones that were spaced such that the uncovered annular areas at the detector were equal (b). The spacing based on equal annular area provided more uniform background intensity. (The increased intensity in the center is due to a small opening in the collimator where the truncated cones did not come to a point.)

described analytically, and it was time-prohibitive to simulate the thousands of variable permutations, so a default set of variables was chosen from which single variables were allowed to deviate. The dimensions of the parallel-hole collimator drove the selection of reasonable default values. Unlike the tungsten parallel-hole collimator, all of the CSH collimators were modeled using lead as the collimator material since it would ease eventual construction and the CSH collimators did not require small unit pitches nor registration with the pixels.

The slant angle of the cones was chosen to fit within the geometric constraints of the MBI system. Because the CSH collimator must be positioned under a lesion, we set the radius of the widest cone to be 4 cm to allow for mobility within the 15×20 cm^2 field-of-view. Allowing for the possibility of a lesion at a distance of 6 cm from the collimator face when using a single-head detector configuration, the maximum cone angle was limited to $\sim 30^\circ$ from vertical.

The distance between the cones was initially chosen to be similar to the spacing of the parallel-hole collimator (1–2 mm). However, it was found that the background uptake was not uniform and increased with increasing diameter. Preliminary simulations showed that the images had more uniform sensitivity when the cones were not spaced evenly but were instead spaced such that the annular area at the base of each cone was equal (Fig. 4). The default area of each annulus was set to 2 cm^2. This area resulted in an average distance between cones of 1.415 mm, approximating the hole diameter of 1.225 mm for the parallel-hole collimator.

The cone wall thickness was set to 0.3 mm and cone height was 1 cm. These values were chosen for ease in modeling while being close to the septal thickness (0.375 mm) and hole length (0.94 cm) of the parallel-hole collimator.

Preliminary simulations showed that some form of septa dividing the area within each cone was required to preserve spatial resolution. Septal spokes were arranged radially every 5°. Initially, septa of constant thickness were modeled, but this resulted in the elimination of active hole area near the center of the CSH collimator. Hence, the septa were simulated as wedges approaching zero width at the center of the collimator (Fig. 5). The default width of the septal wedges at the outer edge of the CSH collimator was set at $1/r^2$, where r is the radius of the outer ring (i.e., a thickness of 0.625 mm at the outer 4 cm radius). This resulted in a median septal thickness of 0.3125 mm, which was similar to the cone thickness of 0.3 mm. The wedge thickness was adjusted by a factor called k. By default, k equaled 1; k values of 0.5 and 2 represented septal wedges that were half and twice as thick as the default wedges, respectively.

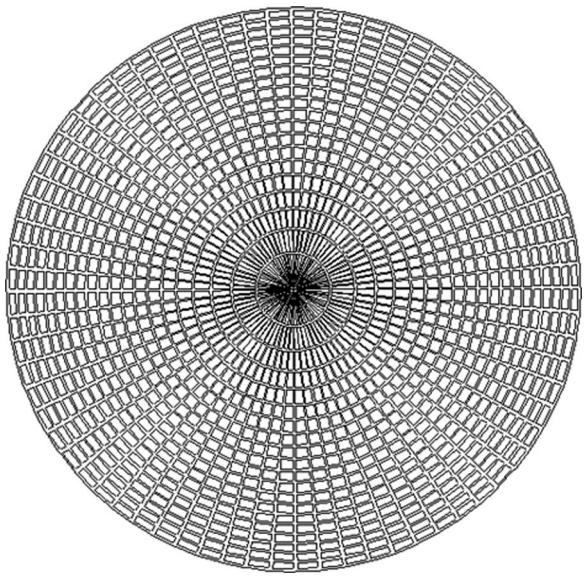

FIG. 5. View of the top of one of the conical slant-hole collimators that was evaluated in the Monte Carlo simulations. Radiating wedge-shaped septa, modeled as infinitely thin at the center, have been inserted every 5°.

The effect of each parameter on collimator performance was investigated by varying each parameter while the remaining parameters were held at the chosen default values. That is, the slant angle was allowed to vary while the other parameters were held to default values; then the annular area was adjusted while the other variables were left unchanged; and so on.

A small number of additional simulations were performed to explore the influence of the lesion characteristics on image quality when using the default CSH collimator parameters. In one simulation, the lesion size was decreased (from 1 to 0.75 cm); in another simulation the lesion depth was shallower (2 rather than 3 cm); and in a third simulation the lesion was offset 5 mm from the center of the CSH collimator. In the last case of the offset lesion, analysis was performed without a correction for the offset, in order to simulate the setting where the collimator was erroneously placed off-center from the lesion.

II.G. Image analysis

The images generated by the various CSH collimator configurations were evaluated using the following measures: accuracy in the determination of lesion depth, spatial resolution as measured by the full width at half maximum (FWHM) of the lesion profile, and count sensitivity. All three parameters were measured from the circumferential count profile of each image. The circumferential count profiles were generated by calculating the radial distance of every pixel from the center pixel. When more than one pixel had the same radial distance from the center pixel, the mean value of the counts in these pixels was determined and used for the profile. The resulting profile of intensity versus radius was smoothed using a Savitzky-Golay smoothing filter.[25]

The lesion depth from the collimator surface, z, was extracted from the peak of the smoothed profile, r_{peak}, according to the trigonometric relationship

$$\tan\theta = \frac{r_{\text{peak}}}{z+h}, \tag{1}$$

where θ is the angle of the cone from vertical and h is the height of the CSH collimator.

The FWHM of each profile was defined by the width of the profile at the intensity halfway between the peak and background intensities. In some instances, the profile at half maximum extended beyond the field-of-view, and the FWHM was then deemed undefined.

Collimator sensitivity was measured from the mean background count density of images that did not contain a lesion. Lesion count sensitivity was measured from the sum of counts in images that contained only the lesion and no background counts.

An ideal collimator should demonstrate accurate depth estimation and a radial profile with a FWHM approaching the lesion size. While meeting these two preferences, an ideal CSH collimator should also retain the greatest sensitivity possible.

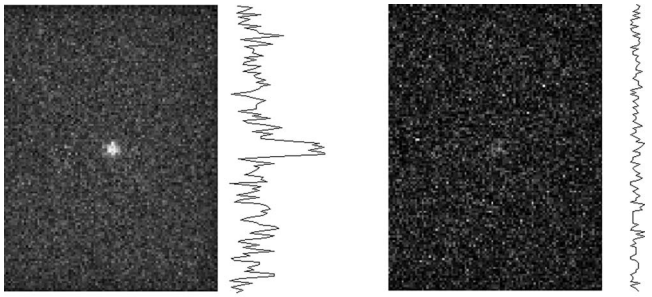

FIG. 6. Simulated images of MBI studies acquired with a parallel-hole collimator. The count densities are equivalent to clinical images performed with 150 MBq Tc-99m sestamibi and acquired for (a) 10 and (b) 1 min. The model included a 6-cm thick breast with a 1-cm diameter lesion located 3 cm from the collimator face. Line profiles through the simulated 1-cm diameter lesion are displayed to the right of each image. FWHM of the lesion profile for (a) was 0.8 ± 0.2 cm. FWHM could not be determined for (b).

III. RESULTS

III.A. Parallel-hole collimator simulations

The simulated 10-min MBI images acquired with the parallel-hole collimator had a count density of 673 counts/cm^2, which was within the desired count density of a clinical 10 min 150 MBq image. For the simulated 1-min image, the count density was 1/10th of that, at 67.3 counts/cm^2.

Figure 6 shows a simulated image of a MBI study performed with 150 MBq Tc-99m sestamibi. A 1-cm diameter lesion was modeled in the center (depth = 3 cm) of a 6-cm thick compressed breast of density 1.0 g/cm^3. Comparison of the 10-min image with the 1-min image shows the impact of noise on image quality and the problem faced when using conventional parallel-hole collimation at low doses and short imaging times. The average FWHM of radial profiles through the lesion in the 10-min image was 0.8 ± 0.2 cm. The 1-min image was too noisy to measure FWHM from profiles through the lesion.

III.B. Conical slant-hole collimator simulations

The default CSH collimator had slightly lower sensitivity than the parallel-hole collimator, with count densities of 635 and 58.6 counts/cm^2 obtained with the 10- and 1-min images, respectively (Fig. 7). The lesion count sensitivity, however, was substantially improved; the number of lesion counts obtained with the default CSH collimator was a factor of 21 greater than that obtained from the parallel-hole collimator (29 000 counts vs 1400 counts in 10 min acquisition).

The lesion depth was estimated from the circumferential profile, and ten separate simulations of the 10-min image resulted in a mean estimated lesion depth of 3.05 cm with a mean FWHM of 2.0 ± 0.1 cm (actual simulated lesion was a 1-cm diameter lesion centered at 3 cm depth), giving an absolute error in depth measurement of 0.5 ± 0.2 mm. The mean absolute error for the 1-min images was worse at 1.1 ± 0.7 mm, and the mean FWHM of the 1-min images was

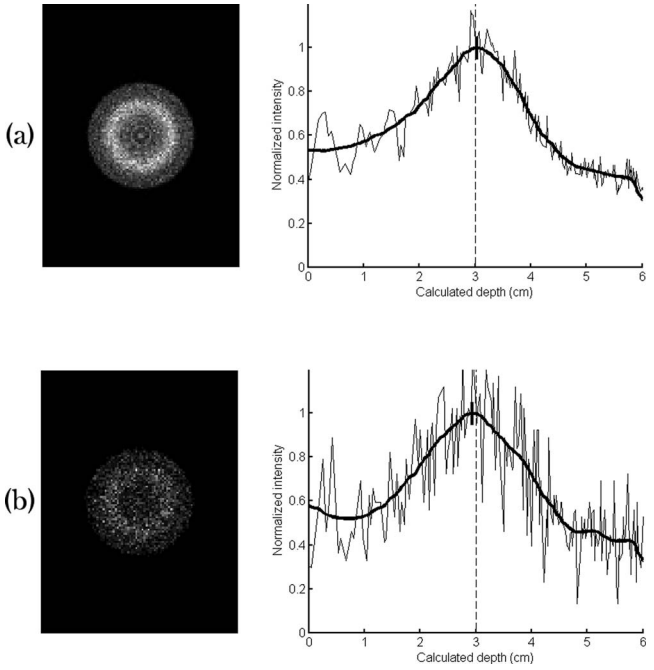

FIG. 7. Simulated images of MBI studies acquired using a conical slant-hole collimator with count densities representing (a) a single 10-min acquisition and (b) a single 1-min acquisition following an injection of 150 MBq Tc-99m sestamibi. The default conical slant-hole collimator parameters were used. The circumferential count profile of each image is displayed at right with the smoothed profile indicated in bold. The depth estimate from the profile is designated by a bold dash at the peak of the profile; the dashed line represents the depth that was actually simulated (3 cm).

2.0 ± 0.2 cm. The smoothed profiles of the ten 1-min frames are shown in Fig. 8. Comparison of the ten individual 1-min profiles illustrates that each run of the 1-min simulation produced similar results. In Figs. 7 and 8, the intensities have been normalized for comparison purposes, and intensity is plotted against the radial distance, which has been converted to depth using Eq. (1).

The effect of changing the five different collimator parameters is displayed through the smoothed circumferential count profiles for each CSH collimator simulated (Figs. 9–13). In Fig. 9, the individual profiles for each slant angle are shown along with the smoothed profile to illustrate both the raw circumferential count profile and the smoothed profile. The estimated depth is again designated for each radial profile as a short line at the peak of the smoothed profile.

Table I details the error in the estimated lesion depth, the FWHM of the 1-cm lesion placed 3 cm from the collimator, and the count sensitivity of each collimator relative to the parallel-hole collimator design.

Cone slant angle (Fig. 9): Fig. 9 and Table I showed a rapid degradation in the determination of lesion depth with decreasing hole angle. As the slant angle decreased, the background count sensitivity increased nearly twofold over the range of 30°–15°, but the FWHM of the radial profiles worsened over twofold and the error of depth estimates increased up to 5.6 mm for the 1-min simulations.

Annular area (Fig. 10): As the annular area increased, the sensitivity increases but the FWHM consistently widened. The depth estimates degraded as well, but the error remained submillimeter for all four annular areas investigated.

Cone wall thickness (Fig. 11): Sensitivity decreased with increasing cone thickness, but the FWHM of the profiles improved. At a thickness of 0.2 mm there was especially poor discrimination between the lesion and its background, which was evident more by the widened FWHM than by the depth estimate.

Cone height (Fig. 12): Sensitivity varied greatest with changes in cone height and tended to decrease as the cone height increased. There was a nearly 2.5-fold increase in counts when the cone height decreased from 1 to 0.75 cm, but the poor FWHM resulted in a radial profile that was not useful for determining the depth of the lesion.

Septal wedge thickness (Fig. 13): Sensitivity decreased as the septal wedges that radiate across the cones were increased in thickness (larger k). Thinner wedges with a smaller coefficient k had flatter radial profiles and worse FWHM values. In general, thicknesses near the default value (i.e., k factor equal to 1) had the best depth estimates, but all errors were submillimeter.

The results from Table I and Figs. 9–13 were used to select parameters that were hypothesized to yield better results through increased sensitivity without substantially compromising accuracy in depth estimation and FWHM. We sought to increase sensitivity through a decrease in angle (from 30° to 25°) and an increase in annular area (from 2.0 to 2.5 cm^2); we attempted to improve depth estimation through an increase in cone thickness (from 0.3 to 0.4 mm); and we fixed the two variables that seemed to be most sensitive to change—cone height and septal wedge thickness—at default values ($h = 1$ cm and $k = 1$). The new design showed a 1.54-fold increase in sensitivity with an absolute error in depth that was still acceptable (2.0 and 1.1 mm for the 10- and 1-min images, respectively) (Fig. 14).

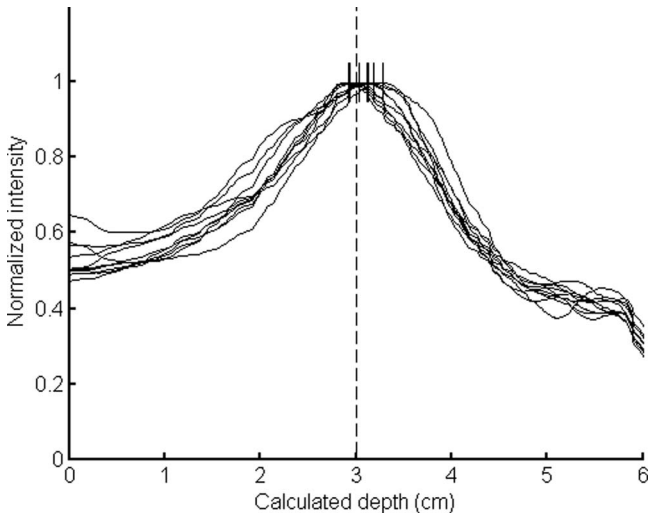

FIG. 8. Plot of ten superimposed smoothed circumferential count profiles generated from the ten 1-min images acquired with the conical slant-hole collimator using default parameters. The estimated depths that were calculated from the images are designated by dashes at the profile peaks. The depth that was actually simulated (3 cm) is indicated with a dashed line.

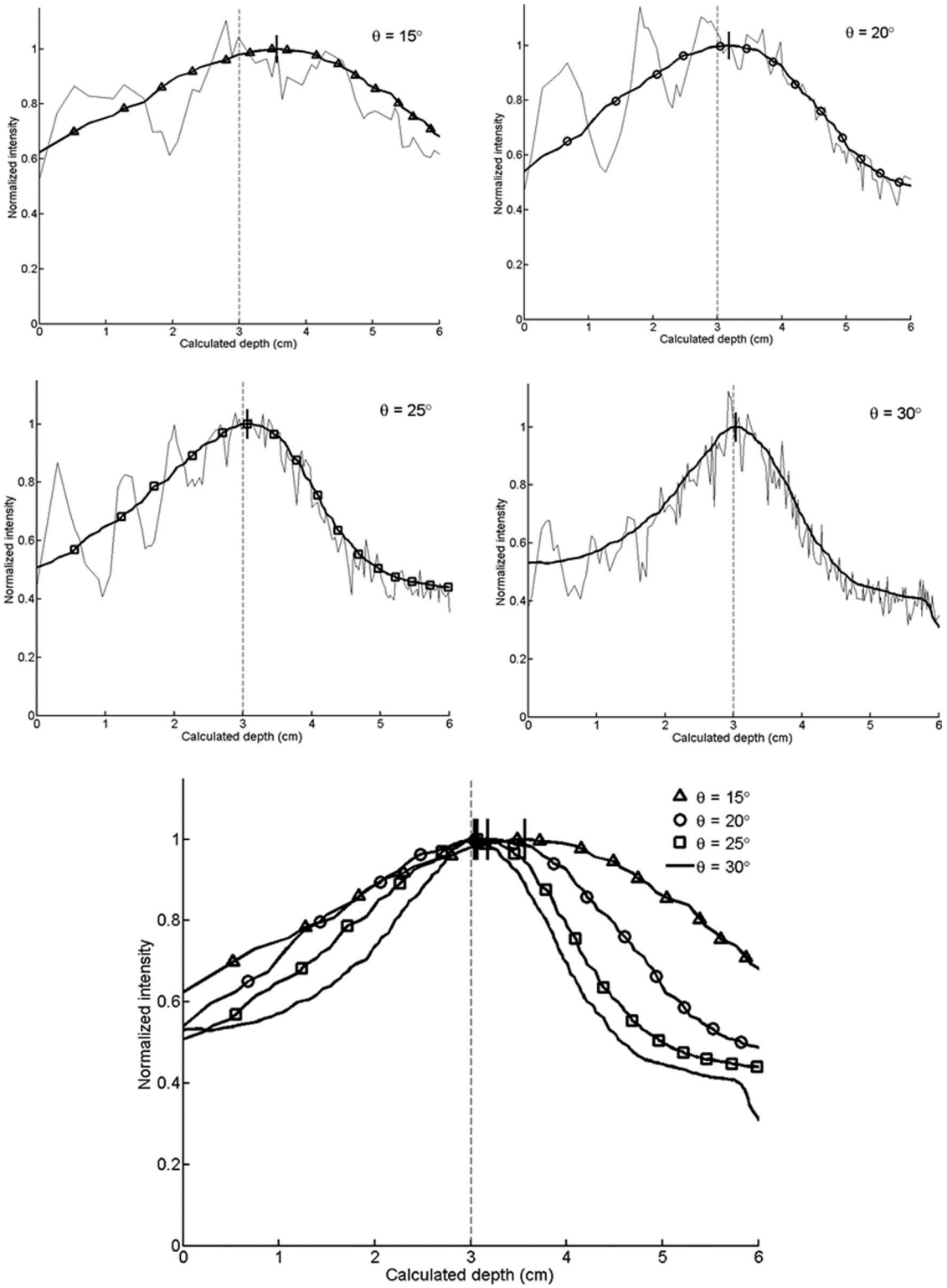

FIG. 9. Circumferential count profiles for conical slant-hole collimators of varying slant angles (θ). The raw and smoothed profiles for each angle are shown at top. The smoothed profiles have been superimposed on the bottom. The calculated depths are designated by dashes at the peaks of the smoothed profiles, with the actual simulated depth of 3 cm indicated by a dashed line.

However, the FWHM degraded from 2.0 to 2.8 cm in the 10-min images.

Image results from the three additional 10-min simulations performed to investigate effects of changes in lesion size and position are shown in Fig. 15. Compared to results from the default CSH collimator, changing the size of the simulated lesion from 1 to 0.75 cm resulted in the same 0.5 mm error in depth estimation and FWHM of 2.0 cm; changing the lesion depth from 3 to 2 cm resulted in increasing error in depth estimation to 2.2 mm but FWHM was unchanged; and changing

TABLE I. Results from Monte Carlo simulations of several conical slant-hole (CSH) collimator designs with varying parameters. The default CSH parameter configuration was $\theta = 30^\circ$, $A = 2$ cm^2, $t = 0.3$ mm, $h = 1$ cm, and $k = 1$, designated by bold. The parameters were allowed to deviate from the default value, with only a single parameter changing in each simulation. Count sensitivity was measured in images of the background only and in images of the lesion only relative to that of the current parallel-hole collimator design. Full-width-at-half-maximum (FWHM) of the circumferential count profile of a 1-cm lesion at 3 cm from the collimator and the absolute error of the estimated lesion depth are reported as the mean ± standard deviation for ten independent simulations that represented image acquisition times of 10 and 1 min.

Variable	Value	Background count at 3 cm sensitivity (relative to parallel-hole design)	Lesion count sensitivity (relative to parallel-hole design)	Absolute error of depth estimate (mm)		FWHM of 1-cm lesion from the collimator (cm)	
				10 min	1 min	10 min	1 min
Angle θ (deg)	**30**	**0.94**	**21.14**	**0.5 ± 0.2**	**1.1 ± 0.7**	**2.0 ± 0.1**	**2.0 ± 0.2**
	25	1.22	11.02	1.3 ± 0.5	1.0 ± 0.7	2.6 ± 0.0	2.7 ± 0.1
	20	1.56	9.84	2.0 ± 0.2	2.0 ± 1.2	3.5 ± 0.1	3.4 ± 0.2
	15	1.91	7.66	5.7 ± 0.5	5.6 ± 1.0	4.3 ± 0.2	4.4 ± 0.6
Area A (cm^2)	1.5	0.62	7.56	0.5 ± 0.2	0.8 ± 0.5	1.8 ± 0.0	1.8 ± 0.2
	2	**0.94**	**21.14**	**0.5 ± 0.2**	**1.1 ± 0.7**	**2.0 ± 0.1**	**2.0 ± 0.2**
	2.5	1.35	14.48	0.4 ± 0.1	1.3 ± 0.8	2.3 ± 0.1	2.5 ± 0.3
	3	1.80	17.72	0.5 ± 0.2	1.5 ± 1.0	2.7 ± 0.2	2.9 ± 0.3
Thickness t (mm)	0.2	1.34	12.58	0.4 ± 0.2	0.8 ± 0.5	2.8 ± 0.7	2.5 ± 0.2
	0.3	**0.94**	**21.14**	**0.5 ± 0.2**	**1.1 ± 0.7**	**2.0 ± 0.1**	**2.0 ± 0.2**
	0.4	0.86	10.20	0.9 ± 0.3	0.7 ± 0.3	1.8 ± 0.1	1.9 ± 0.2
	0.5	0.81	9.60	0.9 ± 0.3	1.2 ± 0.9	1.8 ± 0.0	1.7 ± 0.1
Height h (cm)	0.5	9.60	34.57	21.8 ± 0.2	21.2 ± 0.9	Undefined	Undefined
	0.75	2.44	18.86	1.0 ± 0.3	1.2 ± 0.9	Undefined	Undefined
	1	**0.94**	**21.14**	**0.5 ± 0.2**	**1.1 ± 0.7**	**2.0 ± 0.1**	**2.0 ± 0.2**
	1.25	0.49	6.96	1.7 ± 0.5	1.5 ± 1.1	1.7 ± 0.1	1.7 ± 0.2
Wedge thickness factor k	0.5	1.68	13.25	0.7 ± 0.2	0.9 ± 0.6	Undefined	Undefined
	0.75	1.16	12.00	0.3 ± 0.1	0.9 ± 0.6	2.7 ± 0.7	2.2 ± 0.3
	1	**0.94**	**21.14**	**0.5 ± 0.2**	**1.1 ± 0.7**	**2.0 ± 0.1**	**2.0 ± 0.2**
	1.25	0.82	10.07	0.6 ± 0.3	1.0 ± 0.6	2.0 ± 0.0	2.0 ± 0.2
	1.5	0.72	9.17	0.7 ± 0.3	0.9 ± 0.6	2.0 ± 0.0	1.9 ± 0.2

the position of the lesion such that it was offset 5 mm from the center of the CSH collimator resulted in increasing the error in depth estimation to 5.6 mm and increasing FWHM to 3.4 cm.

IV. DISCUSSION

Our simulations showed that the sensitivity of the CSH collimators trended predictably, increasing when radiation was

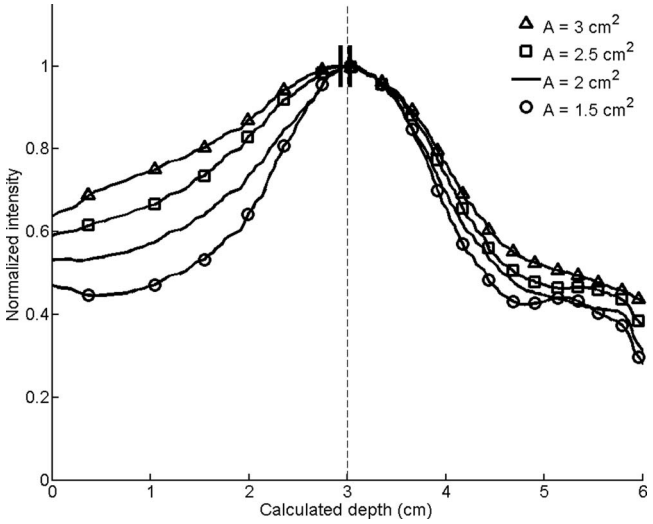

FIG. 10. Smoothed circumferential count profiles for conical slant-hole collimators with varying annular areas (A). The calculated depths are designated by dashes at the peaks of the smoothed profiles, with the actual simulated depth of 3 cm indicated by a dashed line.

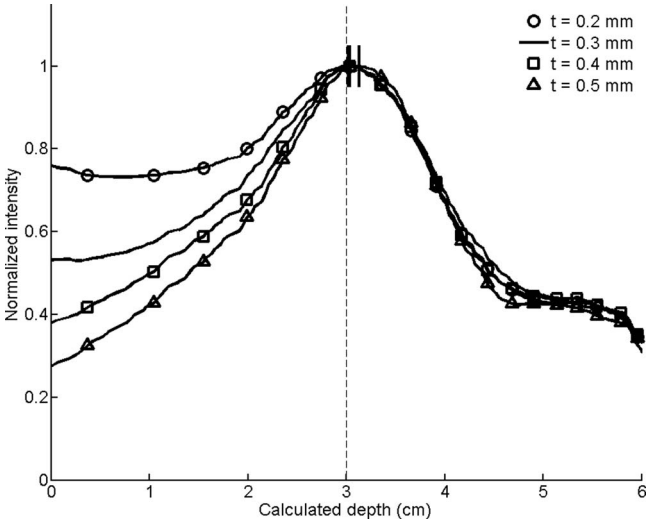

FIG. 11. Smoothed circumferential count profiles for conical slant-hole collimators with varying cone wall thicknesses (t). The calculated depths are designated by dashes at the peaks of the smoothed profiles, with the actual simulated depth of 3 cm indicated by a dashed line.

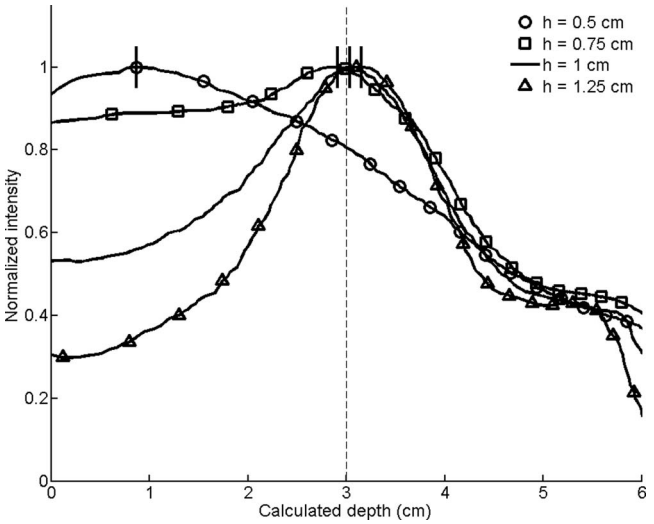

FIG. 12. Smoothed circumferential count profiles for conical collimators with varying cone heights (h). The calculated depths are designated by dashes at the peaks of the smoothed profiles, with the actual simulated depth of 3 cm indicated by a dashed line.

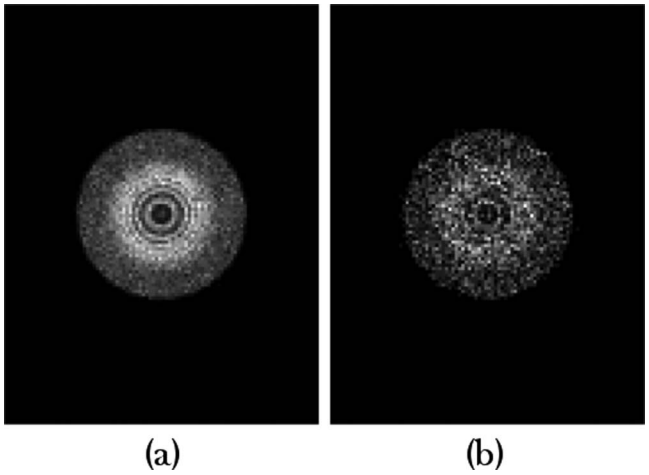

FIG. 14. Simulated images resulting from varying more than one parameter, with the intent to increase sensitivity while maintaining FWHM and absolute error in depth estimation. Variables used were $\theta = 25^\circ$, $A = 2.5$ cm^2, $t = 0.4$ mm, $h = 1$ cm, and $k = 1$. (a) The 10-min image showed a sensitivity of 1.54× the default collimator, depth error of 2.0 mm, and FWHM of 2.8 cm. (b) The 1-min image had a depth error of 1.1 ± 0.7 mm and a FWHM of 2.8 ± 0.2 cm.

impeded by less lead, such as in the cases of smaller hole angles, thinner and shorter cones, and thinner radiating septa. However, despite the increased count density, the resulting images were not always useful, because as expected, FWHM trended in the opposite direction as sensitivity for all parameters. For example, hole angles that are closer to vertical were found to have improved sensitivity but at the expense of decreased resolution and poor depth information. This effect can be seen in the raw profiles of Fig. 9. In the case of the thinner cones and septa, the increased sensitivity derived primarily from increased counts representing background rather than lesion tissue, which increased the count density but worsened lesion detectability. Some of the more dramatic instances of this worsened lesion detectability include the simulations of the thinnest radiating septa ($k = 0.5$) and shortest cone height ($h = 0.5$ cm).

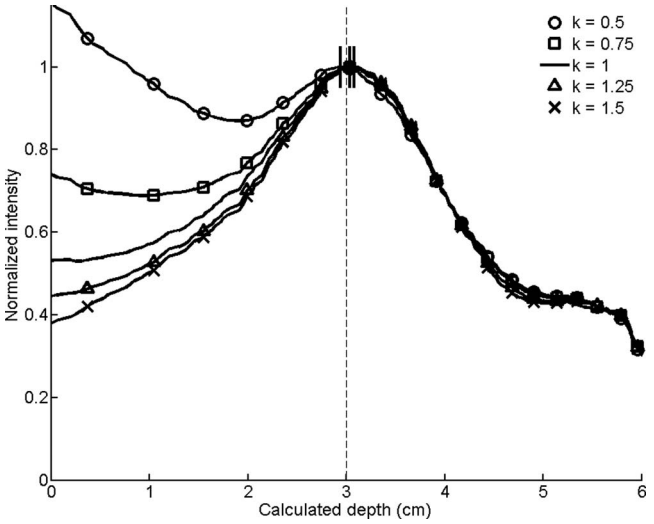

FIG. 13. Smoothed circumferential count profiles for conical collimators with radiating septal wedges of varying thicknesses determined by the coefficient k. The calculated depths are designated by dashes at the peaks of the smoothed profiles, with the actual simulated depth of 3 cm indicated by a dashed line.

It was interesting to note that the smaller hole angles resulted in decreased resolution even though the distance between the detector and lesion was shortest in such cases. We believe that the poorer resolution is a result of the lesion being projected as a smaller ring, which compromised the radial sampling, as seen by poor statistics and increased noise. This effect also contributed to the intensity oscillations observed in the raw profiles of Fig. 9. In addition to the poor sampling rate at pixels nearer the center, the cones are also separated by greater distances when near the center to equalize the annular areas, and it was found that the valleys of the oscillations corresponded to the spacing of the cones of the CSH collimator. At the outer edges of the CSH collimator, the cones are closer together and radial sampling is improved, so the profile becomes less noisy and the intensity oscillations dampen. This improved radial sampling at the outer edge can be useful for biopsy purposes since lesions that are further from the collimator (and in the less noisy portion of the profile) are closer to the opposite side of the breast, so less tissue would need to be traversed during biopsy.

Not only does the wide spacing of the cones near the center cause poorer resolution on that basis alone, but we also discovered that the spacing of the cones near the center of the collimator could be so wide that radiation could enter the detector perpendicularly and further degrade the resolution. Retrospectively, this effect occurred in four of the collimators designs that we evaluated: the two with the most vertical angles ($\theta = 15^\circ$ and 20°) and the two collimators with the shortest hole height ($h = 0.5$ cm and 0.75 cm). These collimator designs consisted of concentric rings with a physical separation of 3.2 mm at the center that decreased to 0.2 mm apart at the outer diameter (mean separation was 1.125 mm).

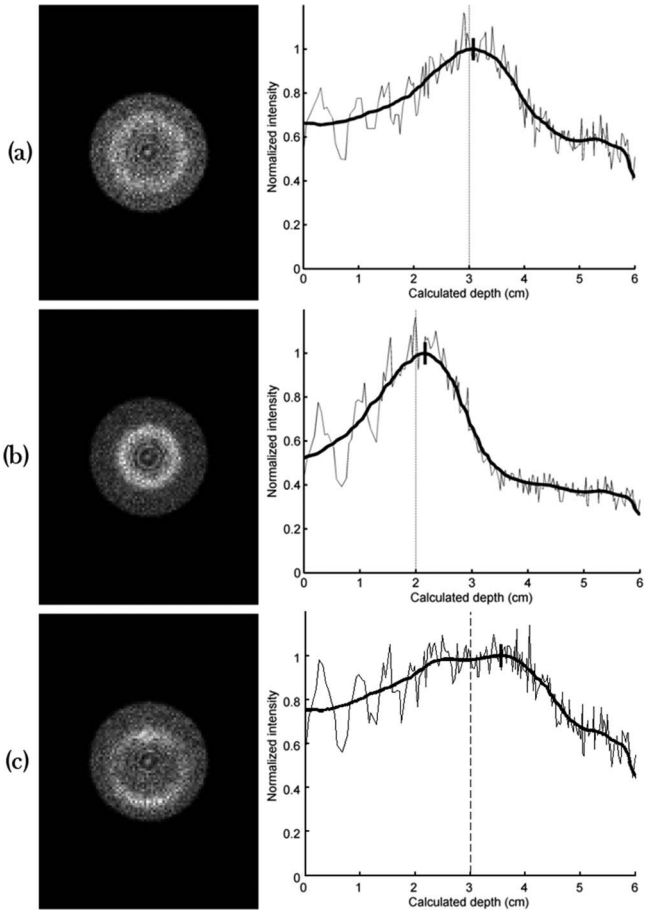

FIG. 15. Simulated 10-min images resulting from changing the lesion's size or position. All images were acquired using the default conical slant-hole collimator parameters. (a) The lesion diameter was decreased from 1 to 0.75 cm. Count sensitivity, error in calculated depth, and FWHM of the circumferential profile were unaffected by this change. (b) The lesion depth was changed from 3 to 2 cm. Error in calculated depth was increased from 0.5 to 2.2 mm with this change; sensitivity and FWHM were unaffected. (c) The lesion was offset 5 mm from the center of the conical slant-hole collimator. Error in calculated depth was increased from 0.5 to 5.6 mm and FWHM was increased from 2.0 to 3.4 cm.

In the simulations, the incident radiation was perpendicular to the collimator surface, partly explaining why these collimators had the two poorest measured FWHM values or undefined FWHM values. The other collimators, including the default CSH collimator, did not experience this effect.

For the lesion simulated (1 cm diameter at 3 cm from the collimator face), it was found that the default CSH collimator parameters were reasonable selections. In the 1-min images, the absolute error in depth estimation was only 1.1 ± 0.7 mm. This error seemed to be acceptable, considering that the lesion was 1 cm in diameter and the sampling notches of biopsy needles are often 1–2 cm in length.

Nevertheless, it is very possible that a selection of slightly different variables may generate a better image. We described a set of CSH collimator parameters that we hypothesized might allow for increased sensitivity while maintaining acceptable FWHM and error in depth estimation. That design did have increased sensitivity ($1.54\times$) but the FWHM of the 1-cm lesion profile was degraded from 2.0 to 2.9 cm. This degradation may be a critical issue for biopsy of small lesions (<1 cm diameter), where the poorer resolution will make it more difficult to visualize the lesion and its location. This emphasizes that the relationship among the parameters is not fully understood, and though the default values are reasonable estimates, the optimal set of parameters for the CSH collimator remains undetermined.

Furthermore, it is likely that the appropriate CSH collimator may differ depending on the size and location of the lesion. We concentrated our efforts on designing a CSH collimator for a lesion that we felt represented a fair and feasible clinical scenario, which was a 1 cm lesion at a depth of 3 cm in a 6 cm breast. Obviously, we were unable to evaluate all possible lesions, but we did consider some basic changes to the lesion description. The imaging results were observed to worsen when the lesion characteristics were changed (Figs. 14 and 15), though part of this is likely because the lesion was changed in manners that made it theoretically less detectable: smaller size, shallower depth such that the lesion resided in the noisier region of the circumferential count profile, and offset from the center of the CSH collimator.

The accuracy of the depth measurement is poorer for lesions close to the collimator. This decreased accuracy is because the lesion is detected through the rings nearest to the center of the collimator. There is greater variability in the circumferential lesion profile because of fewer holes in the center of the collimator to average over, and lesions are not as finely sampled because holes at the center are wider in order to achieve uniform annular area.

If different CSH collimators prove to lend themselves to certain lesions, then a lesion's characteristics, such as size, depth, and intensity, could be roughly estimated from preliminary planar MBI imaging, and the CSH collimator best suited to the lesion could be used. As for the offset of the lesion relative to the CSH collimator center, the offset would be observed as a relatively intact but shifted ring of intensity (Fig. 15), which would be relatively easy to correct through repositioning and imaging feedback.

In this work, we simulated the situation of a single lesion in the breast. In the clinical setting, it is possible that more than one sestamibi-avid lesions may be present and the obtained imaging would not be a single ring but overlapping rings, making a more complex image. In our experience in detection of new lesions on MBI, nearly every case is of a single small lesion that could not be visualized with diagnostic mammography or targeted ultrasound. For cases with multiple lesions that would be considered for MBI-guided biopsy, we envision that the breast would be positioned such that maximum separation between lesions is obtained. If multiple lesions are present in close proximity of one another, the chance that they will all be occult on targeted ultrasound, prohibiting ultrasound-guided biopsy is extremely unusual.

Despite establishing the theoretical feasibility of a focused collimator for biopsy purposes, the practicality of manufacturing such a collimator is uncertain. The radial septal wedges would be unnecessary once the wedge thickness fell below a

minimum value, as the small cone diameter would eliminate the need for them. At small cone diameters, they could be eliminated or replaced with varying numbers of small radial bars spaced between the cone rings. The construction of the cone rings themselves should not prove challenging, as they can all be cut from a single cone. A problem arises when lesions are close to the edge of the detector field of view, such as lesions near the chest wall. In those cases, the CSH collimator cannot be positioned directly under the lesion. A compromise for such cases would be to construct the collimator in two halves. Both halves would be placed together for normal use and one half could be used for chest wall lesions, although with the reduced sensitivity, it would require twice the imaging time to estimate lesion depth.

Further work will be required to develop the entire biopsy system. The design will require that the conventional collimator be replaced with a collimator tray that can hold either the CSH collimator or a standard parallel-hole collimator of the same size. The tray must be movable in both the x- and y-dimensions to allow positioning beneath a lesion. By using a tray design, we can accommodate different CSH collimators, as alternative designs may be required for patients with very large or small breasts.

An important issue not addressed here is tracking of the location of the biopsy needle during the biopsy process. The most attractive approach is the use of a radioactive obturator, using a radiotracer such as I-125 that can be visualized without interfering with the image of the lesion. With the CSH collimator design described above, we believe that we can develop a biopsy system that will enable close to real-time visualization of the lesion and obturator. One of the main benefits of a short imaging time is the ability to detect any shift of the lesion within the breast during the biopsy process. Occasionally, the process of introducing the biopsy needle or patient motion may result in the lesion being shifted. Rapid feedback to the radiologist regarding a change in lesion location is important in recognizing the problem. In addition, acquisition of images before, during, and after the biopsy will allow the operator to quantitate changes in lesion activity, thereby enabling the radiologist to confirm that tissue from the lesion was successfully obtained.

A shorter imaging time could further be accomplished by increasing the administered dose. This work showed promising results for a simulated dose of 150 MBq Tc-99m sestamibi, which is the target dose in our laboratory for routine clinical MBI studies performed in the screening setting. A one-time increased dose for biopsy purposes could consequently be permissible and would aid in accurate and rapid imaging. Use of an administered dose as much as 740 MBq Tc-99m sestamibi would permit very rapid imaging at a radiation dose equivalent to or less than that currently employed with breast specific gamma imaging (740-1111 MBq Tc-99m sestamibi) and positron emission mammography (PEM) (~370 MBq F-18 FDG). These other technologies already deliver an increased radiation dose and are consequently limited in their ability to reduce biopsy imaging time through administration of higher radiopharmaceutical doses. Work from our institution has demonstrated ability perform MBI using 150-300 MBq Tc-99m sestamibi due to several count sensitivity improvement methods such as registered high sensitivity collimation and use of a wide energy window for CZT detectors.[23,24]

Another advantage of the CSH collimator design is that the single-detector configuration would permit easier access to the breast than is possible with PEM, which requires a dual-detector configuration for positional information. Depending on the gantry design, a single-detector configuration would allow for theoretically infinite choices in positioning around the breast to optimize visualization and access to the lesion.

V. CONCLUSION

This work used a Monte Carlo model to demonstrate the feasibility of a conical slant-hole collimator design for rapid biopsy application in molecular breast imaging. Specifically, lesion depth of a 1-cm diameter lesion positioned in the center of a typical breast can be estimated with error of less than 2 mm (average error of 1.1 ± 0.7 mm) using circumferential count profiles of images acquired in 1 min. The collimator dimensions can be reasonably selected by emulating an optimized parallel-hole collimator design. Future work includes constructing a collimator tray, adjusting the collimator parameters to facilitate manufacturing of an actual CSH collimator, and engineering the MBI gantry to permit incorporation of the biopsy system.

ACKNOWLEDGMENTS

This research was supported by Mayo Clinic Foundation and a grant National Institutes of Health (NIH) (R21R33 CA 128407). The Mayo Foundation and three authors of this work (A. L. Weinmann, C. B. Hruska, and M. K. O'Connor) obtain royalties from licensing arrangements between the Mayo Foundation and Gamma Medica-Ideas.

[a]Author to whom correspondence should be addressed. Electronic mail: hruska.carrie@mayo.edu; Telephone: 507-284-9599; Fax: 507-266-4461.

[1]W. A. Berg, I. N. Weinberg, D. Narayanan, M. E. Lobrano, E. Ross, L. Amodei, L. Tafra, L. P. Adler, J. Uddo, W. Stein, III, and E. A. Levine, "High-resolution fluorodeoxyglucose positron emission tomography with compression ("positron emission mammography") is highly accurate in depicting primary breast cancer," Breast J. **12**, 309–323 (2006).

[2]R. F. Brem, J. M. Schoonjans, D. A. Kieper, S. Majewski, S. Goodman, and C. Civelek, "High-resolution scintimammography: A pilot study," J. Nucl. Med. **43**, 909–915 (2002).

[3]M. K. O'Connor, S. W. Phillips, C. B. Hruska, D. J. Rhodes, and D. A. Collins, "Molecular breast imaging: Advantages and limitations of a scintimammographic technique in patients with small breast tumors," Breast J. **13**, 3–11 (2007).

[4]D. J. Rhodes, C. B. Hruska, S. W. Phillips, D. H. Whaley, and M. K. O'Connor, "Dedicated dual-head gamma imaging for breast cancer screening in women with mammographically dense breasts," Radiology **258**, 106–118 (2011).

[5]C. B. Hruska, D. J. Rhodes, D. A. Collins, C. L. Tortorelli, J. W. Askew, and M. K. O'Connor, "Evaluation of molecular breast imaging in women undergoing myocardial perfusion imaging with tc-99m sestamibi," J. Womens Health **21**, 730–738 (2012).

[6]R. F. Brem, J. A. Rapelyea, G. Zisman, K. Mohtashemi, J. Raub, C. B. Teal, S. Majewski, and B. L. Welch, "Occult breast cancer: Scintimammography with high-resolution breast-specific gamma camera in women at high risk for breast cancer," Radiology **237**, 274–280 (2005).

[7]W. A. Berg, K. S. Madsen, K. Schilling, M. Tartar, E. D. Pisano, L. H. Larsen, D. Narayanan, A. Ozonoff, J. P. Miller, and J. E. Kalinyak, "Breast cancer: Comparative effectiveness of positron emission mammography and MR imaging in presurgical planning for the ipsilateral breast," Radiology **258**, 59–72 (2011).
[8]W. A. Berg, K. S. Madsen, K. Schilling, M. Tartar, E. D. Pisano, L. H. Larsen, D. Narayanan, and J. E. Kalinyak, "Comparative effectiveness of positron emission mammography and MRI in the contralateral breast of women with newly diagnosed breast cancer," AJR, Am. J. Roentgenol. **198**, 219–232 (2012).
[9]A. L. Conners, C. B. Hruska, C. L. Tortorelli, R. W. Maxwell, D. J. Rhodes, J. C. Boughey, and W. A. Berg, "Lexicon for standardized interpretation of gamma camera molecular breast imaging: Observer agreement and diagnostic accuracy," Eur. J. Nucl. Med. Mol. Imaging **39**, 971–982 (2012).
[10]C. Pletta, C. Hruska, D. Rhodes, and M. O'Connor, "Impact of diagnostic workup resulting from a positive low-dose molecular breast imaging scan in a screening environment," J. Nucl. Med. **52**, 2301 (2011) (Meeting Abstracts).
[11]W. A. Berg, J. D. Blume, A. M. Adams, R. A. Jong, R. G. Barr, D. E. Lehrer, E. D. Pisano, W. P. Evans, III, M. C. Mahoney, L. H. Larsen, G. J. Gabrielli, and E. B. Mendelson, "Reasons women at elevated risk of breast cancer refuse breast MR imaging screening: ACRIN 6666," Radiology **254**, 79–87 (2010).
[12]B. Welch, R. Brem, B. Kross, V. Popov, R. Wojcik, and S. Majewski, "Gamma-guided stereotactic breast biopsy system,"IEEE Trans. Nucl. Sci. **53**, 2690–2697 (2006).
[13]L. R. Coover and P. J. Malaspina, "Breast tumor localization using sestamibi," Clin. Nucl. Med. **27**, 161–164 (2002).
[14]L. R. Coover, G. Caravaglia, and P. Kuhn, "Scintimammography with dedicated breast camera detects and localizes occult carcinoma," J. Nucl. Med. **45**, 553–558 (2004).
[15]I. Khalkhali, F. S. Mishkin, L. E. Diggles, and S. R. Klein, "Radionuclide-guided stereotactic prebiopsy localization of nonpalpable breast lesions with normal mammograms," J. Nucl. Med. **38**, 1019–1022 (1997).
[16]J. E. Kalinyak, K. Schilling, W. A. Berg, D. Narayanan, J. P. Mayberry, R. Rai, E. B. Dupree, D. K. Shusterman, M. A. Gittleman, W. Luo, and C. G. Matthews, "PET-guided breast biopsy," Breast J. **17**, 143–151 (2011).
[17]B. L. Welch, C. Lorino, D. Chiarella, T. Hodge, "Clinical use of a stereotactic breast-specific gamma imaging apparatus in the localization of breast lesions for biopsy [abstract]," J. Nucl. Med. **52**, 675 (2011).
[18]C. B. Hruska and M. K. O'Connor, "Quantification of lesion size, depth, and uptake using a dual-head molecular breast imaging system," Med. Phys. **35**, 1365–1376 (2008).
[19]Los Alamos Monte Carlo Group, *MCNP- A General Monte Carlo N-Particle Transport Code Version 5* (Radiation Safety Information Computational Center at Oak Ridge National Laboratory (CCC-740), 2003).
[20]A. L. Weinmann, C. B. Hruska, and M. K. O'Connor, "Design of optimal collimation for dedicated molecular breast imaging systems," Med. Phys. **36**, 845–856 (2009).
[21]C. B. Hruska, S. W. Phillips, D. H. Whaley, D. J. Rhodes, and M. K. O'Connor, "Molecular breast imaging: use of a dual-head dedicated gamma camera to detect small breast tumors," AJR, Am. J. Roentgenol. **191**, 1805–1815 (2008).
[22]C. B. Hruska and M. K. O'Connor, "Effect of collimator selection on tumor detection for dedicated nuclear breast imaging systems," IEEE Trans. Nucl. Sci. **53**, 2680–2689 (2006).
[23]C. B. Hruska, A. L. Weinmann, and M. K. O'Connor, "Proof of concept for low-dose molecular breast imaging with a dual-head CZT gamma camera. Part I. Evaluation in phantoms," Med. Phys. **39**, 3466–3475 (2012).
[24]C. B. Hruska, A. L. Weinmann, C. M. Tello Skjerseth, E. M. Wagenaar, A. L. Conners, C. L. Tortorelli, R. W. Maxwell, D. J. Rhodes, and M. K. O'Connor, "Proof of concept for low-dose molecular breast imaging with a dual-head CZT gamma camera. Part II. Evaluation in patients," Med. Phys. **39**, 3476–3483 (2012).
[25]A. Savitzky and M. J. E. Golay, "Smoothing and differentiation of data by simplified least squares procedures," Anal. Chem. **36**, 1627–1639 (1964).